**ARCHIVES OF TRANSPORT** ***ISSN (print):*** *0866-9546*
*Volume 64, Issue 4, 2022* ***e-ISSN (online):*** *2300-8830*
***DOI:*** *10.5604/01.3001.0016.1229*

# RESEARCH ON AGV POSITIONING METHOD COMBINED WITH IMU AND UWB

**Jiandong QIU[1], Yang ZHANG[2], Minan TANG[3], Panpan MA[4], Jiajia RAN[5]**

[1, 2, 4, 5] *School of Mechanical Engineering, Lanzhou Jiaotong University, Lanzhou, China*

[3] *School of Automation Electrical Engineering, Lanzhou Jiaotong University, Lanzhou, China*

## *Abstract:*

*Aiming at the problem that automated guided vehicle (AGV) is difficult to locate accurately due to the influence of environment and time drift when it works in the indoor intelligent storage system. In this paper, an extended kalman filtering (EKF) framework is designed. In order to make full use of the original ranging values of ultra wideband (UWB) and inertial measurement unit (IMU), the framework realizes the fusion positioning between UWB module and IMU module in a tight coupling manner, so as to ensure that the system can still work when the available base station signal is inaccurate. Firstly, for the problem that the traditional UWB positioning method is easily affected by the non-line of sight (NLOS) error indoors, the calculated positioning coordinate value is unstable. With the help of different NLOS probability distribution curves of different obstacles, the weighted least square method is applied to the UWB positioning method to determine the positioning coordinate value of UWB, which improves the sudden change of AGV positioning coordinate in the static environment. Then the data fusion algorithm is optimized, and the error value of IMU and UWB coordinate is taken as the observation value of EKF, which reduces the influence of cumulative error on IMU positioning results, provides the global optimal estimation of the system optimal state, and improves the fusion positioning accuracy. Finally, the measured data of UWB and IMU systems in indoor complex environment are simulated in MATLAB. The experimental results show that when NLOS signal seriously affects the positioning effect, the UWB and IMU combined positioning system can provide more reliable positioning results than the single IMU positioning system. It improves the positioning accuracy of AGV and provides a new idea for indoor positioning mode.*

***Keywords:*** *intelligent storage system, extended kalman filter, AGV, data fusion positioning, inertial navigation*

## *To cite this article:*

*Qiu, J., Zhang, Y., Tang, M., Ma, P., Ran, J. (2022). Research on AGV positioning method combined with IMU and UWB. Archives of Transport, 64(4), 107-117. DOI: https://doi.org/10.5604/01.3001.0016.1229*

**Contact:**
1) qiujd@mail.lzjtu.cn [https://orcid.org/0000-0001-9972-898X]; 2) 563448563@qq.com [https://orcid.org/0000-0001-6995-293X]; 3) tangminan@mail.lzjtu.cn [https://orcid.org/0000-0003-1424-2708] – corresponding author; 4) 210772234@qq.com [https://orcid.org/0000-0002-6876-2330]; 5) 1170910995@qq.com [https://orcid.org/0000-0001-9674-4079]

*Article is available in open access and licensed under a Creative Commons Attribution 4.0 International (CC BY 4.0)*

## 1. Introduction

In recent years, due to the rapid development of intelligent and unmanned manufacturing industry, many logistics companies and manufacturing factories have introduced intelligent warehousing system as a practical means to improve production efficiency and reduce operating costs. The intelligent storage system makes full use of various mechanical and transportation equipment, computer systems, integrated operation coordination and other technical means. Through the overall planning and application of the logistics system, efficient access to goods can be achieved. To achieve the purpose of saving effort, being efficient, reasonable, fast, efficient, accurate and reliable in logistics related operations and contents (Sun et al., 2014). Intelligent storage system is an intelligent system composed of three-dimensional shelves, track roadway stacker, in and out transportation system, information identification system, automatic control system, computer monitoring system, computer management system and other auxiliary equipment (Liu et al. 2021; Michlowicz. 2021). Because intelligent storage has the characteristics of high informatization and automation, control optimization algorithm has become the soul of intelligent storage (Ding et al., 2018). At present, the intelligent warehousing optimization algorithm is mainly focused on AGV. Because of its flexibility, intelligence, and other characteristics, AGV has become an important part of workshop logistics and has been widely used (Ning et al. 2020). As a key link to realize the automatic transportation of materials and goods in an intelligent factory, the autonomous positioning of AGV is very important, because it is the premise to realize the functions of path planning, autonomous obstacle avoidance and so on (Ding et al. 2018; Uradzinski et al. 2017). The research and development of accurate and reliable AGV positioning method can not only improve the convenience and accuracy of target positioning, but also have strong engineering value and practical significance.

There are many kinds of navigation and positioning methods for mobile robots, mainly including visual navigation and positioning, electromagnetic navigation and positioning, GPS global positioning, light reflection navigation and positioning (Jiang et al. 2012), etc. These positioning methods use different sensors and cooperate with the robot motion, so that the robot can achieve high-precision positioning and navigation under the constraints of different environments. Among them, laser rangefinders are more convenient than other technologies to perceive the characteristics of complex environments, and have better accuracy and lower computational complexity. Common indoor positioning technologies include Radio Frequency Identification (RFID), ultra wideband (UWB), Wireless Fidelity(Wi-Fi), ZigBee, radar, etc. Oulose et al. (2019) uses ZigBee technology for indoor positioning. Although it has strong penetration ability, the positioning environment is limited. This positioning method is easy to be interrupted by the magnetic field generated in the surrounding environment. In addition, the hardware deployment is also very complex. The positioning accuracy of this method is only about 1m. Wang et al. (2019) studied the application of IMU in indoor positioning, and proposed a method to suppress the cumulative error of IMU in the positioning process by using the complementary output data of magnetometer and gyroscope. The maximum estimation error under rectangular trajectory is 2.6m, while the error under linear trajectory is only 1.2m. Although the result is improved compared with the traditional method, the actual accuracy is still not ideal. Ai et al. (2017) proposed a UWB location algorithm to enhance asymmetric bilateral bidirectional ranging for indoor target location and tracking, with a location accuracy of about 0.17m, but the experiment did not consider the introduction of environmental interference and other factors. This is an ideal positioning environment, which cannot be directly applied in the actual engineering environment. Although UWB has high positioning accuracy and can provide centimeter level ranging accuracy, there are complex electromagnetic environment and indoor obstacles (walls, partitions, equipment, etc.) in the indoor environment. Under NLOS conditions, whether these obstacles weaken or absorb the UWB signal, the final positioning will be affected (Zhou et al. 2021). The existing methods to eliminate NLOS errors mainly focus on two aspects. On the one hand, we try to model the unknown NLOS and reconstruct the measurements that are not affected by it. On the other hand, measurement information from other sensors or scene related prior map knowledge are introduced to compensate for errors caused by NLOS (Cao et al., 2022; Yin et al., 2021). IMU has strong anti-interference capability, high updating rate of

real-time navigation data, and strong stability. However, it is still very difficult to locate for a long time due to the accumulated errors. Therefore, a single location and navigation method can not meet the needs of complex indoor scene applications. In the actual complex working environment, how to combine the advantages of various positioning methods to obtain better positioning effect is a problem that needs to be discussed in this paper. Aiming at the above problems, the proposed solution is to make full use of the positioning advantages of UWB and IMU sensors to obtain more accurate and robust positioning results. The main contribution of this paper is that, in practical application scenarios, due to the uncertainty of NLOS, the improved weighted least squares method is used for UWB positioning to obtain static AGV coordinate data. It improves the existing NLOS model, which is difficult to adapt to various interference situations. Then, use IMU to obtain real-time AGV coordinate information. The EKF framework is used to fuse multi-sensor information, input the data of each subsystem to the information fusion center, and process multiple data. It ensures the full use of information and the accuracy of AGV position information output, and improves the reliability of system measurement data.

## 2. Optimization of UWB Wireless ranging and positioning method

### 2.1. Traditional ultra wideband wireless ranging and positioning

There are usually many positioning algorithms based on wireless signals, which can be divided into ranging and non-ranging (Yang et al. 2021). The ranging and positioning algorithm used in this paper calculates and estimates the distance between nodes by using the spatial connectivity and signal transmission of nodes. The two-way ranging mode is the commonly used ranging mode, and the ranging algorithm is the trilateral positioning algorithm (Zhang et al. 2021). The ranging model between the mobile tag and the base station at time t can be expressed as:

$$D_i(t) = L_i(t) + L_{i,NLOS}(t) + n_{r,i}(t) \qquad i = 1,2,\ldots,m,(m \le 3) \quad (1)$$

In Formula 1, $D_i(t)$ represents the actual distance measurement value, $L_i(t)$ represents the actual distance, $L_{i,NLOS}(t)$ represents the NLOS error term, and $n_{r,i}$ represents the Gaussian white noise generated in the measurement process.

After the relative distance of each point is obtained by using equation (1), the specific location of the target is determined by using the three base station positioning method in Figure 1. Obviously, the location of the target is located at the intersection of three circles with the radius of the length from the three base stations to the target. Therefore, theoretically, as long as the three known base stations are not on the same straight line, the result of distance location of the three base stations is unique.

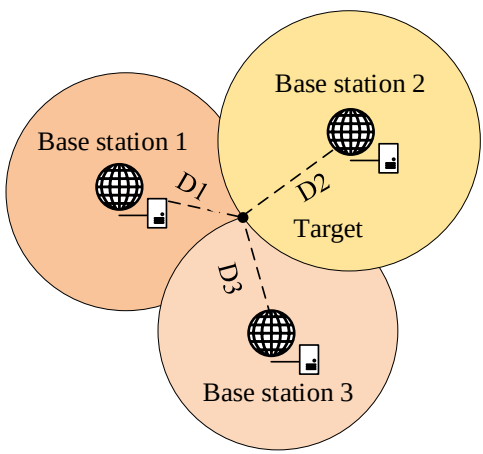


Fig. 1. location mode of three base stations

Assume that the unknown label coordinates are $(X,Y)$ and the distance from it to each base station $(X_i, Y_i)$ is $D_i$. Where $i$ should be less than the number of base stations, so the difference between the measured distance and the actual distance can be represented by $\rho_i = \dot{D}_i - D_i$ Then determine $(X,Y)$ by the value of least square $\sum_{i=1}^{n} \rho_i^2$. That is, each distance can determine an equation about the location of the known reference base station and the unknown base station, as shown in equation (2).

$$\begin{cases} D_1 = \sqrt{(X - X_1)^2 + (Y - Y_1)^2} \\ D_2 = \sqrt{(X - X_2)^2 + (Y - Y_2)^2} \\ D_3 = \sqrt{(X - X_3)^2 + (Y - Y_3)^2} \\ \vdots \\ D_i = \sqrt{(X - X_i)^2 + (Y - Y_i)^2} \end{cases} \tag{2}$$

After simplifying $D_i$-$D_{i-i}$ in equation (2), the desired target position value is obtained.

$$\begin{bmatrix} X_2 - X_1 & Y_2 - Y_1 \\ X_3 - X_1 & Y_3 - Y_1 \\ \vdots & \vdots \\ X_i - X_1 & Y_2 - Y_1 \end{bmatrix} \begin{bmatrix} X \\ Y \end{bmatrix} = \frac{1}{2} \begin{bmatrix} X_2^2 - Y_2^2 - D_2^2 - (X_1^2 + Y_1^2 - D_1^2) \\ X_3^2 - Y_3^2 - D_3^2 - (X_1^2 + Y_1^2 - D_1^2) \\ \vdots \\ X_i^2 - Y_i^2 - D_i^2 - (X_1^2 + Y_1^2 - D_1^2) \end{bmatrix} \tag{3}$$

$$\mathbf{H} = \begin{bmatrix} X_2 - X_1 & Y_2 - Y_1 \\ X_3 - X_1 & Y_3 - Y_1 \\ \vdots & \vdots \\ X_i - X_1 & Y_2 - Y_1 \end{bmatrix} \tag{4}$$

$$\mathbf{B} = \frac{1}{2} \begin{bmatrix} X_2^2 - Y_2^2 - D_2^2 - (X_1^2 + Y_1^2 - D_1^2) \\ X_3^2 - Y_3^2 - D_3^2 - (X_1^2 + Y_1^2 - D_1^2) \\ \vdots \\ X_i^2 - Y_i^2 - D_i^2 - (X_1^2 + Y_1^2 - D_1^2) \end{bmatrix} \tag{5}$$

Then the target position coordinates in equation (3) are shown in equation (6):

$$\begin{bmatrix} X \\ Y \end{bmatrix} = \left(\mathbf{H}^T \mathbf{H}\right)^{-1} \mathbf{H}^T \mathbf{B} \tag{6}$$

### 2.2. UWB Positioning Method Based on Weighted Least Squares

The least square method used in the above settlement process is to calculate the coordinate position without distinguishing the weights of all ranging values and give the same weight value (Xu et al. 2018). However, in the actual production and application process, there are different obstacles between each base station and the tag, which also leads to the different degree of NLOS error received by each ranging value. The error size of the obstacles in the distance between each base station and the tag should be determined, and the ranging value with small error should be given a relatively large weight, and the ranging value with large error should be given a relatively small weight. This paper proposes a method to reduce the error impact of NLOS on ranging by obtaining the NLOS probability distribution curve of different obstacles, giving different weights to the error size caused by different positions between different base stations and obstacles, and then using the least square method (Yu et al. 2019; Jiang et al. 2021).

NLOS error expression 7 based on bidirectional ranging is as follows:

$$\Delta d = \frac{10(\sqrt{\varepsilon_{nlos} - 1})}{att_{nlos}} \lg\left( \frac{\max_{1 \le i \le L}\left(a_i^2 \tau_i^{\eta}\right)}{a_{DP}^2 \tau_{DP}^{\eta}} \right) \tag{7}$$

Where $\varepsilon_{nlos}$ and $att_{nlos}$ respectively represent the dielectric constant related to the obstacles encountered by the signal in the propagation path and the attenuation factor of the corresponding obstacles, $L$ is the number of current base stations, $a_i$and $\tau_i$ represent the maximum distance value and the time value required to pass through the $i$-th path.

According to equation (7), NLOS error changes correspondingly with the change of the material of different obstacles. Using different signal channels to sample and compare UWB can reduce the estimated NLOS error, and compare different sampling values with the actual values to obtain more accurate NLOS error values. Specifically, in the sampling process, the measured error value of each channel is subdivided into $w$ intervals. The frequency of the midpoint on the $i$-th interval and the error value monitored in this area are $a_k$ and $b_k$ respectively, which are brought into the normal distribution curve for linear fitting to obtain the error distribution curve under each channel. Among them, it is assumed that the NLOS error of each channel follows a normal distribution, which is shown in equation (8) after sampling and fitting $m$ different channels:

$$\min_{A_j, \bar{x}_j, \delta_j} \sum_{i=1}^{w} \left( f_j\left(a_k\right) - b_k \right)^2, j = 1, 2, ..., \mathrm{m} \tag{8}$$

In equation (8), $f(x)$ is specifically expressed as:

$$f(x)=\frac{A_j}{\sqrt{2\pi}\sigma_j}e^{\frac{(x-\bar{x}_j)^2}{2\sigma_j^2}} \tag{9}$$

There are many ways to solve nonlinear optimization problems in numerical calculation, among which the most effective is the quasi Newton method (Jiang et al. 2017). The specific step is to calculate the gradient value of the objective function at each iteration, and obtain the probability distribution curve of NLOS error under different channels by solving the above formula.

Finally, bring the obtained NLOS error probability value into equation 10, and the target position is:

$$\begin{bmatrix} X \\ Y \end{bmatrix}=\left(\mathbf{H}^T\boldsymbol{\beta}\mathbf{H}\right)^{-1}\mathbf{H}^T\boldsymbol{\beta}\mathbf{B} \tag{10}$$

$$\boldsymbol{\beta}=\begin{pmatrix} \beta_1 & 0 & 0 \\ 0 & \beta_2 & 0 \\ 0 & 0 & \beta_i \end{pmatrix} \tag{11}$$

## 3. IMU positioning mode

The inertial navigation system is based on the principle of inertia. It does not need any external information, nor does it radiate any information outward. The inertial navigation system alone can independently and covertly carry out continuous positioning and orientation in the world and in any medium environment under all-weather conditions (Liang et al. 2021). The inertial navigation system has built-in three-axis accelerometer and three-axis gyroscope, which are used to measure the angular motion information and linear motion information of the carrier respectively. The airborne computer calculates the heading, attitude, speed and position of the carrier based on these measures information.

The calculation process of inertial navigation includes attitude update, speed update and position update, and its differential equation is (17).

$$\dot{\mathbf{Q}}=\frac{1}{2}\mathbf{Q}\otimes\boldsymbol{\omega}_{nb}^{b} \tag{12}$$

$$\dot{\mathbf{V}}=\mathbf{C}_{\mathbf{b}}^{\mathbf{m}}f^{b}-(2\boldsymbol{\omega}_{\mathbf{ie}}^{\mathbf{n}}+\boldsymbol{\omega}_{\mathbf{en}}^{\mathbf{n}})\times\mathbf{V}+g^{n} \tag{13}$$

$$\dot{\mathbf{P}}=\mathbf{V}-\boldsymbol{\omega}_{\mathbf{en}}^{\mathbf{n}}\times\mathbf{P} \tag{14}$$

Where $\boldsymbol{Q}$ is the quaternion of the carrier attitude. $\boldsymbol{\omega}_{nb}^{n}$ is the projection of angular velocity in the carrier coordinate system, which can be obtained from equation (14). $\boldsymbol{\omega}_{ib}^{n}$ is the output value of the inertial

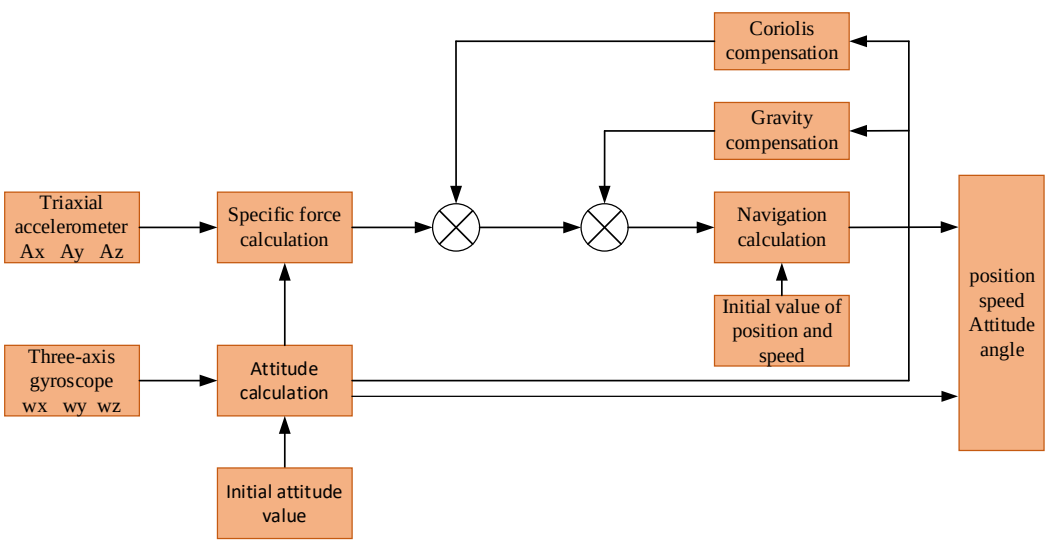


Fig. 2. Structure diagram of IMU attitude calculation algorithm

navigation gyroscope. $\mathbf{C_b^m}$ is the state transfer moment from the carrier coordinate system to the navigation coordinate system. $\boldsymbol{\omega}_{\mathbf{en}}^{\mathbf{n}}$ and $\boldsymbol{\omega}_{\mathbf{ie}}^{\mathbf{n}}$ are the position rate and rotation rate respectively, for the conversion of the navigation coordinate system to the earth coordinate system, see equation (16); $f^b$ is the specific force of acceleration on the carrier; $g^n$ is the local gravitational acceleration; $\boldsymbol{V}$ and $\boldsymbol{P}$ is respectively the speed and position of the carrier in the navigation coordinates.

$$\boldsymbol{\omega}_{nb}^{b} = \boldsymbol{\omega}_{ib}^{b} - C_b^n(\boldsymbol{\omega}_{ie}^{n} + \boldsymbol{\omega}_{en}^{n}) \tag{15}$$

$$\boldsymbol{\omega}_{ie}^{n} = \begin{bmatrix} \boldsymbol{\omega}_{ie}\cos L & 0 & -\boldsymbol{\omega}_{ie}\sin L \end{bmatrix}^{\mathrm{T}} \tag{16}$$

$$\boldsymbol{\omega}_{en}^{n} = \begin{bmatrix} \dfrac{V_e}{R_N+H} & \dfrac{-V_n}{R_M+H} & \dfrac{-V_e}{R_N+H}\tan L \end{bmatrix}^{\mathrm{T}} \tag{17}$$

## 4. Location algorithm of UWB and IMU information fusion

### 4.1. EKF System Structure

Compared with Wi-Fi, Bluetooth, ZigBee and other indoor wireless positioning technologies, although UWB signal has the advantages of high resolution, centimeter ranging accuracy and so on. However, due to the high complexity of the indoor environment and many obstacles, the signal may encounter non line of sight, multi-path and other problems in the transmission process (Jiang et al. 2021). The IMU positioning mode has the outputted track estimation information, which has high positioning accuracy in a short time and is not affected by the non-line of sight environment. Based on the above considerations, this paper designs a UWB and IMU fusion positioning method based on EKF technology, and uses the respective advantages and characteristics of these two sensors to improve the accuracy of the system in the output coordinates. Specifically, when the indoor NLOS error is large, inertial navigation is used to minimize the error caused by environmental interference in UWB, and the advantage of UWB high-precision ranging is used to suppress the cumulative error in the process of inertial navigation solution. There are two kinds of fusion location methods: loose coupling and tight coupling, in which loose coupling is relatively simple. The two systems involved in the fusion positioning are independent of each other in the positioning process. Only the two sets of positioning results obtained are simply fused. On the contrary, tight coupling is a relatively advanced fusion method. In the process of positioning solution, the information obtained by the two systems is fused, and the two are fully used to make it an integrated positioning method. In this paper, the tight coupling fusion method is used to combine UWB ranging data with inertial navigation data to reduce the positioning error.

In this paper, EKF is applied to the tight coupling combined positioning of IMU system and UWB. The functional block diagram of UWB ranging and IMU system tight coupling fusion positioning is shown in Figure 3.

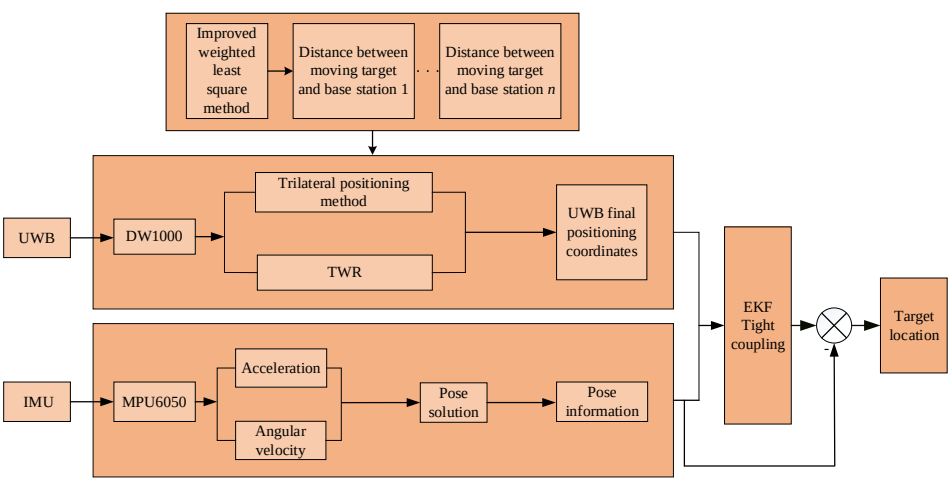


Fig. 3. Tight coupling combined positioning system of IMU and UWB

### 4.2. Determination of each state value in EKF algorithm

In this paper, the AGV working condition only involves plane motion, so only the changes of *X* and *Y* axes are considered. Under the tight coupling scheme, the error value of the position and speed of the *X* and *Y* axes solved by the IMU subsystem is taken as the space state vector value of the system, That is, at time *k*, the state vector of the system is $\mathbf{X_k} = \begin{bmatrix} \delta v_x & \delta v_y & \delta p_x & \delta p_y \end{bmatrix}^T$, the predictive state equation of the system can be expressed as:

$$\mathbf{X_{k+1}} = \mathbf{F}\mathbf{X_k} + \mathbf{W}_k \tag{18}$$

Where $\boldsymbol{W_k}$ is the state noise of the system. Moreover, $\mathbf{W}_k \sim N(0, \mathbf{Q_k})$, $\boldsymbol{F}$ is the state transition matrix of the system, which can be expressed as:

$$\mathbf{F} = \begin{bmatrix} 1 & 0 & 0 & 0 \\ 0 & 1 & 0 & 0 \\ \Delta t & 0 & 1 & 0 \\ 0 & \Delta t & 0 & 1 \end{bmatrix} \tag{19}$$

Where $\Delta t$ is the sampling period of the system.

In a tightly coupled system, the observed value is different from the value of the state quantity. The difference between the positioning value of the output UWB and the positioning value of the IMU output is taken as the measured value of the system, and finally corrected in combination with the output of the IMU subsystem.

The observed value at time *k* is:

$$\mathbf{Z_k} = \begin{bmatrix} (D_{1,k}^{IMU})^2 - (D_{1,k}^{UWB})^2 \\ (D_{2,k}^{IMU})^2 - (D_{2,k}^{UWB})^2 \\ \vdots \\ (D_{n,k}^{IMU})^2 - (D_{n,k}^{UWB})^2 \end{bmatrix} \tag{20}$$

The distance between the subsystem IMU and the *i*-th base station node at time *k* can be expressed as:

$$D_{i,k}^{IMU} = \sqrt{\left(p_{x,k}^{IMU} - x_i\right)^2 - \left(p_{y,k}^{IMU} - y_i\right)^2} \tag{21}$$

The distance between the AGV mobile tag node and the *i*-th base station node can be expressed as:

$$D_{i,k}^{UWB} = \sqrt{\left(p_{x,k} - x_i\right)^2 - \left(p_{y,k} - y_i\right)^2} + \varepsilon \tag{22}$$

It can be obtained that the observation vector at time *k* is $\mathbf{Z_k}$, which includes the true distance $H(X_k)$ from the tag to the base station and the distance observation noise $\mathbf{V_k}$. then the observation equation of the system can be obtained as follows:

$$\mathbf{Z_k} = H(X_k) + \mathbf{V_k} \tag{23}$$

Where $H(X_k)$ represents the nonlinear observation function of the observation equation with respect to the real distance, $\mathbf{V_k}$ represents the observation noise of the system, and the observation noise obeys $\mathbf{V_k} \sim N(0, \mathbf{R_k})$, and $\mathbf{R_k}$ is the observation noise covariance matrix of the system. By first-order Taylor expansion of the observed value and ignoring the remainder above the quadratic term, the Jacobian matrix **H(k)** at time *k* can be obtained as:

$$\mathbf{H(k)} = \begin{bmatrix} 0 & 0 & \frac{\partial D_1(k)}{\partial x(k)} & \frac{\partial D_1(k)}{\partial y(k)} \\ 0 & 0 & \frac{\partial D_2(k)}{\partial x(k)} & \frac{\partial D_2(k)}{\partial y(k)} \\ \vdots & \vdots & \vdots & \vdots \\ 0 & 0 & \frac{\partial D_n(k)}{\partial x(k)} & \frac{\partial D_n(k)}{\partial y(k)} \end{bmatrix} \tag{24}$$

$$\begin{cases} \frac{\partial D_i(k)}{\partial x(k)} = 2\left(p_{x,k}^{IMU} - x_i\right) - 2\delta p_{x,k} \\ \frac{\partial D_i(k)}{\partial y(k)} = 2\left(p_{y,k}^{IMU} - y_i\right) - 2\delta p_{y,k} \end{cases} \tag{25}$$

## 5. Experimental results and analysis

### 5.1. UWB static experiment

In order to verify the performance of UWB system, an indoor positioning scene is simulated, which is assumed to be 6m×5m room, the lower left corner is

the origin, and a rectangular row is set. There are four base stations in total. Each vertex of the box is equipped with a base station, and the center is equipped with a base station. Its location coordinates are shown in Table 1.

Table 1. Detailed list of base station coordinates

| Base station serial number | Northbound coordinates (m) | Easterly coordinates (m) | Vertical coordinates (m) |
|---|---|---|---|
| 1 | 0 | 0 | 1.5 |
| 2 | 0 | 6 | 1.5 |
| 3 | 5 | 0 | 1.5 |
| 4 | 5 | 6 | 1.5 |

Within the coverage range of the reference node, place the labels on different points, and calculate the coordinates of 10 times of UWB ranging information through STM32. Assuming that the AGV speed is 0.5m/s, the noise error follows N~(0,0.042), the ranging error of the UWB positioning system under LOS follows N~(0,0.0262), and the NLOS distribution is N~(0.114, 0.145), the AGV static coordinates are calculated. The results are compared with the traditional trilateral positioning method, as shown in Table 2.

### 5.2. Fusion algorithm experiment

In order to further verify the positioning performance of the positioning algorithm proposed in this paper, a positioning system platform integrating IMU and UWB is built independently. The parameters of each sensor are shown in Table 3. In the experiment, the two hardware are installed in the center of AGV, and the system diagram is shown in Figure 4. The specific coordinates of each UWB base station are shown in Table 4. Using the above system, the experiment was conducted in 20m×40m space.

Fig. 4. Picture of AGV used in the experiment

Table 3. The system uses various parameters of the sensor

| | UWB-S1-SMA-TCXO | ATK-MPU6050 |
|---|---|---|
| Power supply interface | USB-5V | USB-5V |
| Output interface | USB communication | USB communication |
| Detection distance | STM32F103 | STM32F103 |
| Main control chip | 80m | / |
| Ranging accuracy | ±5cm | 0.01° |

Table 4. Detailed list of base station coordinates

| Base station serial number | Northbound coordinates (m) | Easterly coordinates (m) | Vertical coordinates (m) |
|---|---|---|---|
| 1 | 0 | 0 | 1.5 |
| 2 | 0 | 20 | 1.5 |
| 3 | 40 | 0 | 1.5 |
| 4 | 40 | 20 | 1.5 |

Table 2. Comparison of positioning errors under NLOS error mean

| Serial number | True coordinate value/m | Average coordinate/m | | RMSE/m | | Percentage increase |
|---|---|---|---|---|---|---|
| | | Traditional trilateral positioning method | Weighted least square location method | Trilateral positioning error | Weighted positioning error | |
| 1 | (0.6,0.6) | (0.805,0.431) | (0.718,0.517) | 0.2817 | 0.1471 | 47.76% |
| 2 | (0.6,0.27) | (0.707,0.248) | (0.661,0.281) | 0.2592 | 0.1272 | 50.92% |
| 3 | (0.6,4.8) | (0.653,4.392) | (0.707,4.515) | 0.4328 | 0.2885 | 33.34% |
| 4 | (1.8,4.8) | (1.831,4.267) | (1.848,4.550) | 0.5458 | 0.2584 | 52.65% |
| 5 | (3.0,4.8) | (3.262,4.269) | (3.148,4.563) | 0.6173 | 0.3057 | 50.47% |

The experimental scenario is as follows: when $t$=0, take the location tag to be tested in the base station coordinate system and take the coordinates (0, 0) as the starting point, and the AGV trolley moves slowly along the established uniform linear path from the static state at the speed of 0.1m/s. After the UWB location information and IMU location information are calculated through the STM32 control board on the AGV, the proposed tight coupling algorithm is used for data fusion processing. Finally, the processed data drawing is used for comparative analysis by MATLAB 2014b software.

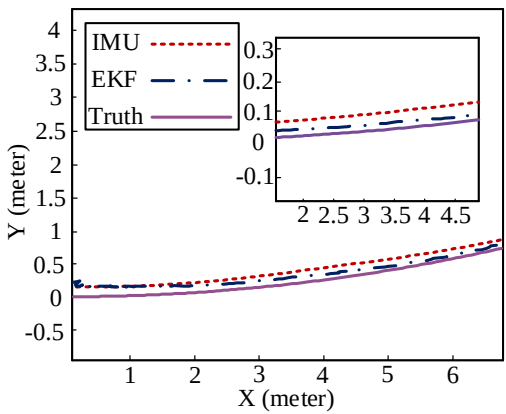


Fig. 5. Comparison of short-time fusion positioning trajectories

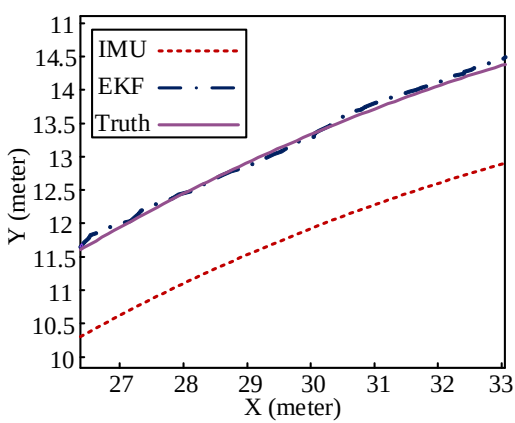


Fig. 6. Comparison of long-time fusion positioning trajectories

It can be seen from Figure 5 that there is little difference between the trajectory of the tightly coupled EKF method and the IMU at the beginning of operation. After a period of time, it can be clearly seen that the IMU trajectory deviates from the real trajectory, while the trajectory of the tightly coupled EKF method is highly consistent with the real trajectory.

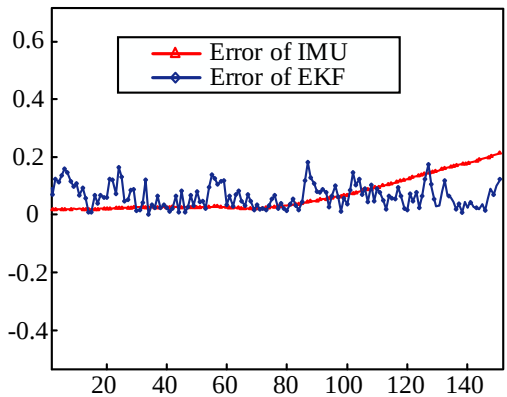


Fig. 7. short time positioning error curve

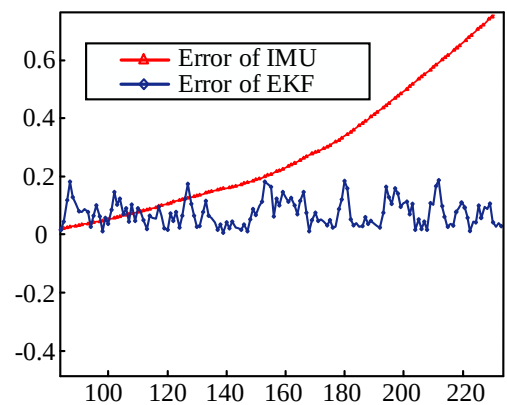


Fig. 8. long time positioning error curve

After about 220 Monte Carlo experiments. It can be seen from the comparison curve of IMU and EKF positioning errors in Figure 8. At 20 times, due to the influence of NLOS error of UWB, the RMSE of the location method of closely coupled EKF is 0.039. Compared with IMU's RMSE of 0.043m, this has little advantage. It can be seen from Figure 6 that in 200 experiments, the RMSE of the EKF positioning method remains within the range of 0 to 0.2.

However, the error of the IMU increases exponentially. In 200 experiments, the RMSE of the EKF positioning method used in the experiment is 0.185 higher than that of the traditional IMU positioning method, which is 56.92% higher than that of the single use.

Table 5. RMSE comparison between dynamic measurement and real value

| Serial number | RMSE | | Percentage increase |
|---|---|---|---|
| | Error of IMU | Error of EKF | |
| 20 | 0.043 | 0.039 | 9.32% |
| 100 | 0.093 | 0.087 | 8.42% |
| 150 | 0.124 | 0.117 | 8.43% |
| 200 | 0.325 | 0.134 | 56.92% |

## 6. Conclusion

Positioning technology is one of the key technologies of AGV. In recent years, integrated positioning technology has attracted much attention, and has strong advantages in anti-interference and improving positioning accuracy.

According to the designed optimization method of combined positioning, the values of single IMU and this method are compared. In the static state, when there is NLOS error interference in the room, the coordinate value determined by the positioning system proposed in this paper is 47.02% higher than before. Under dynamic conditions, the root mean square error value of the combined structure and filtering method adopted by the system in the 100th Monte Carlo experiment is 0.087, 8.42% higher than that of a single IMU, 0.139 in the 200th experiment, 56.92% higher than that of a single IMU.

The experimental results show that the system runs stably and realizes the long-term continuous and reliable positioning.

## References

[1] Ai, H., Li, Y. (2017) Weighted centroid location algorithm based on RSSI ranging filter optimization. *Journal of the Computer Engineering and Design*,3811(10), 2631-2635.

[2] Cao, B., Wang, S. B., Ge, S. R. (2022) Research on positioning strategy and technology of shearer end based on ultra wideband system. *Journal of the Coal Science and Technology*, 50(03), 257-266.

[3] Ding, L., Zhang, Y., Yin, S. C., et al. (2018) Discussion on the development status and trends of my country's logistics and storage industry. *Journal of the Hoistingand Conveying Machinery*, (4), 69−71

[4] Jiang, W., Cao, Z, J., Lu, D, B., et al. (2021) UWB enhanced integrated navigation method under GNSS constraints. *Journal of the Railway Transaction*, 43(03), 111-119.

[5] Jiang, W., Cao, Z. J., Lu, D. B., et al. (2021) UWB enhanced integrated navigation method under GNSS constraints. *Journal of the Railway Transaction*, 43(03), 111-119.

[6] Jiang, W., Li, Y., Rico, Z., et al. (2017) Seamless Indoor-outdoorNavigation based on GNSS , INS and Terrestrial Ranging Techniques. *Journal of the Navigation*, 70(6), 1183-1204.

[7] Jiang, X., Zhang, H., Wei, W., et al.(2012) NLOS error mitigation with information fusion algorithm for UWB ranging systems. *Journal of the China Universities of Posts and Telecommunications.* 19(2), 22-29.

[8] Li, K. P., Liu, T. B., He, B. Q., et al. (2022) Research on AGV path planning and scheduling in "goods to people" picking system. *Journal of the Chinese Management Science*, 30(04), 240-251.

[9] Li, S., Yuan, Z, G., Wang, C., et al. (2018) A survey of swarm intelligence algorithms for optimizing support vector machine parameters. *Journal of the Intelligent Systems*, 13(1), 70-84.

[10] Liang, Y., Zhang, Q, D., Zhao, Ning., et al. (2021) Indoor positioning method based on fusion of UWB and inertial navigation. *Journal of the Infrared and Laser Engineering*, 50(09), 293-306.

[11] Liu, Q. L., Wang, Z. P., Zhou, W. M., et al. (2021) An improved indoor location method based on multi-source information fusion. *Journal of the Telecommunication Engineering*, 61(12), 1526-1533.

[12] Michlowicz, E. (2021) Logistics engineering and industry 4.0 and digital factory. *Journal of the Archives of Transport*, 57(01), 59-72. DOI: https://doi.org/10.5604/01.3001.0014.7484.

[13] Ning, Y. S., Li, Q. S., Lu, P. H., et al. (2020) Collaborative optimization algorithm of

intelligent storage location planning and AGV path planning. *Journal of the Software*, 31(09), 2770-2784.

[14] Oulose, A., Eyobu, S., Han, D. S., et al. (2019) An indoor position estimation algorithm using smartphone IMU sensor data. *Journal of the IEEE Access*, 7(8), 11165-11177.

[15] San, M., Cortes, A., (2020) Precise positioning of autonomous vehicles combining UWB rangingestimations with on-board sensors. *Journal of the Navigation Electronics*, 9(8), 1238.

[16] Uradzinski, M., Guo, H., Liu, X., et al. (2017) Advanced indoor positioning using Zigbee wireless technology. *Journal of the Wireless Personal Communications*, 97(67), 6509-6518.

[17] Wang, C. Q., Feng, D. Q., He, C. L., et al. (2019) Research on enhanced asymmetric bilateral bidirectional ranging algorithm based on UWB. *Journal of the Nanchang Aeronautical University*, 33(01), 66-73.

[18] Xu, Y. L., Zheng, Z. W., Sun, L., et al. (2018) Multi sensor fusion PDR location method based on Neural Network. *Journal of the Sensing Technology*, 31(04), 579-587.

[19] Yang, G., Zhu, S. L., Li, Qiang., et al. (2021) Firefighter indoor location and NLOS detection algorithm integrating UWB and IMU. *Journal of the Computer Engineering*, 47(09), 153-161.

[20] Yin, K. Y., Liang, W., Yang, J. B., et al. (2021) An efficient UWB and IMU fusion localization algorithm in power operation scenarios. *Journal of the China Power*, 54(08), 83-90.

[21] Yu, K., Wen, K., (2019) A novel NLOS mitigation algorithm for UWB localization in harsh indoor environments. *Journal of the IEEE Transactionson Vehicular Technology*, 68(1), 686-699.

[22] Zhang, D. C., Wei, G. L., Tian, X., et al. (2019) Dynamic updating channel model positioning system based on particle filter in NLOS environment. *Journal of the Small Microcomputer System*, 40(12), 2608-2613.

[23] Zhang, Y. D., Tian, L., Li, M. Q., et al.(2017) Application research and demonstration of intelligent patrol robot system in thermal power industry. *Journal of the China Power*, 50(10), 1-7.

[24] Zhou, J., Wei, G. L., Tian, X., et al. (2021) A new indoor location algorithm integrating UWB and IMU data. *Journal of the Small Microcomputer System*, 42(08), 1741-1746.